Quantitative Electron Tomography of Rubber Composites

Lech Staniewicz[1], Thomas Vaudey[2], Christophe Degrandcourt[2], Marc Couty[2], Fabien Gaboriaud[2] and Paul Midgley[1]

[1] Department of Materials Science and Metallurgy, University of Cambridge, Pembroke Street, Cambridge, CB2 3QZ, UK
[2] Manufacture Française des Pneumatiques Michelin, 23 Place des Carmes Déchaux, 63040 Clermont Ferrand Cedex 9, France

E-mail: ltls2@cam.ac.uk

Abstract.

Rubber composite materials have many applications, one example being tyre manufacture. The presence of a filler material in the composite (such as carbon black or silica) causes its mechanical properties to differ in several ways when compared to pure rubber such as viscoelastic behaviour (the Payne effect), increased tensile strength and improved wear resistance. To fully understand these properties, it is necessary to characterise how the filler material is organised on the nanoscale. Using composite materials representative of those found in tyres, this work illustrates the use of electron tomography and machine learning methods as tools to describe the percolation behaviour of the filler; in this case, we focus on the largest proportion of particles absorbed into one single object as a function of particle spacing.

1. Introduction

The change in the mechanical properties of a rubber-filler composite material with the concentration of filler particles was first characterised by Payne in 1962 [1]. He demonstrated that the bulk modulus increased with both the quantity of filler particles in the composite and the effective surface area of the filler particles themselves. Filler particles will form a percolating network when the quantity present in the material exceeds a certain threshold, as shown by a sudden rise in electrical conductivity [2] at the threshold filler concentration. The mechanical properties of a rubber composite show a dependency on the filler concentration [3, 4] with a similar percolation transition - implying that there is a critical distance between filler particles before an electrical or mechanical network can be formed.

The structural properties of rubber-filler composites are key issues in designing new materials. As these composites are heterogeneous, bulk measurements of the volume fraction alone are not sufficient and local, nanoscale information is necessary to fully understand these materials and their properties. Electron tomography enables a complete 3D volume of a nanoscale object to be reconstructed and can provide quantitative structural information from this volume.

Previous work [2] has emphasised the percolation structure of filler particles by skeletonising networks of particles. In contrast, this work is intended to determine what proportion of the filler contributes to the percolation network by measuring the distribution of particle spacings.

Content from this work may be used under the terms of the Creative Commons Attribution 3.0 licence. Any further distribution of this work must maintain attribution to the author(s) and the title of the work, journal citation and DOI.
Published under licence by IOP Publishing Ltd

2. Experimental Methods

5 μm long, 100–150 nm diameter cylindrical pillars were fabricated from rubber composite samples using an FEI Helios FIB/SEM dual-beam instrument and mounted on Omniprobe TEM grids. Pillars were imaged in an FEI Tecnai F20 instrument at 200 kV under HAADF STEM conditions (detector collection angle of 23.7–118 mrad) using a pixel size of 0.56 nm, a dwell time of 11.7 μs and an image size of 1024x1024 pixels (field of view: 573x573 nm). A tilt series was recorded using the FEI Xplore3D software from -76° to $+76^\circ$ with automatic focus and manually-assisted tracking. Tilt series were aligned using cross-correlation and reconstructed using 20 iterations of the SIRT algorithm [5] with the FEI Inspect3D software.

3. Data Processing and Results

Because the exact shape of each filler particle is intimately linked to the inter-particle spacings, it is important that the reconstruction is not biased in any post-processing operation. Although image filters such as anisotropic diffusion may improve the contrast and make it easier to delineate the boundaries of filler particles, these operations may change the position of the particle boundaries and introduce inaccuracies into any measurements made.

Unfortunately, SIRT reconstructions are not 3-level images. The voxel intensity values for each component (vacuum, rubber, filler) overlap and so a simple thresholding algorithm will not provide an accurate distinction between particle and matrix. Figure 1 illustrates the effect of a 3-level Otsu thresholding operation carried out on one "Z-slice" of a tomographic reconstruction, along with one example of mis-classification.

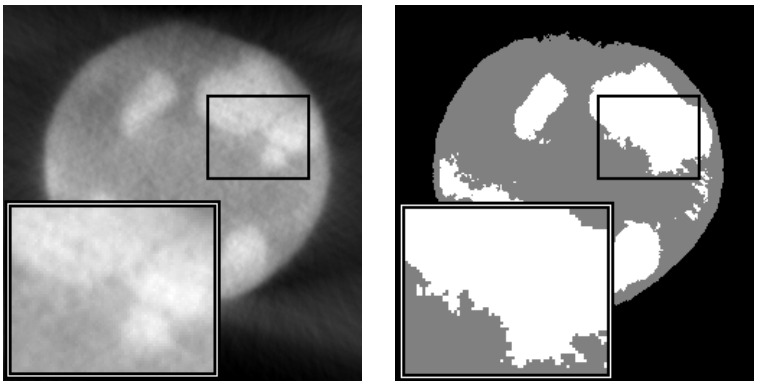

(a) (b)

Figure 1: The results of running a 3-level Otsu thresholding algorithm (b) on an unprocessed reconstruction (a). Inset regions are 2x magnified - the raw data is visibly more concave than the Otsu-thresholded area. Pillar diameter = 110 nm.

A more accurate option is to have a trained operator go over each image and manually delineate parts of the image as belonging to a specific phase. While a human operator can easily work around uneven particle intensities (such as in Figure 1), manual classification is time-consuming, susceptible to operator bias and will not give identical results when repeatedly applied to the same data due to human error.

Machine learning tools can be used to find a compromise between these two extremes. They function by having the user mark portions of the unchanged source image as belonging to one specific class or phase, just as in manual image classification. The software is then taught to recognise those phases by analysing the marked regions on "feature" images which are generated by running image filters (such as gradient operations and smoothing) on the source image. Some form of decision algorithm is then used to identify the un-marked parts of the image (and other images, if operating on an image stack) as belonging to one of the defined classes and a map is created from this information. Any mis-classifications can be corrected and the procedure repeated until the operator is satisfied with the result. Because the original image is used as the reference for the human operator to compare and correct mistakes against and because multiple filtered images are taken together to obtain a result, any applied filtering operations should not alter the quantitative nature of the data.

This method offers a combination of the potential accuracy of a trained human operator with the repeatability of an automated routine (the classification data can be saved for later use). Training the software, although much faster than manually marking out every particle in a reconstruction image stack, can be time consuming. Classifier training on this reconstruction took approximately 16 hours of operator time, including processing time for the software.

This work uses a machine learning package called Trainable Weka Segmentation, implemented in the freely-available Fiji software [6]. It offers a choice from multiple decision algorithms and feature image - we used the default random forest algorithm [7] with the following features: Gaussian Blur and Difference of Gaussians (feature size detection); Sobel filter, Laplacian filter, Derivatives, Gabor filter, Structure Tensor, Membrane Projections and Hessian Matrix (edge detection); and Variance, Anisotropic Diffusion, Bilateral filter, Kuwahara filter, Entropy and Neighbours (pixel intensity detection).

Since the entire feature stack is held in memory while training, using such a large number of features requires a great deal of RAM. Therefore, training is carried out on a substack consisting of every 15th image in the reconstruction, taken along the pillar axis. The pillar reconstruction used in this work is 250x250x950 voxels in size and the training procedure on a 1-in-15 substack consumed approximately 10 GB of RAM. Applying the final classifier to the full reconstruction took approximately 6 hours of processing time on an Intel Core i7-2600 CPU and used substantially less RAM, since each image slice is calculated separately.

Figure 2 shows the results of a trained classifier on the same data as in figure 1. The classified image appears to match the raw data much more accurately than with global thresholding. Since the source image has remained unchanged, there is no ambiguity as to whether any filtering process has altered the data and so the results can be considered accurate enough for pixel-level quantification.

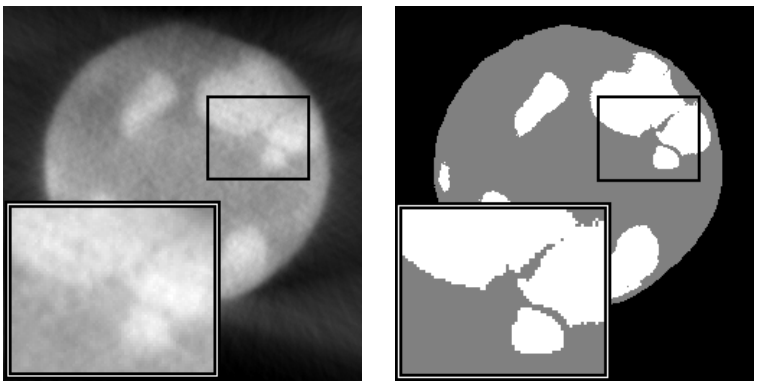

(a) (b)

Figure 2: The same reconstruction as in Figure 1, but processed with the Trainable Weka Segmentation software. Inset region is the same as in Figure 1. Pillar diameter = 110 nm.

The classified data is then segmented and percolated. Percolation is quantified by the closest approach distance between two particles and the degree of percolation by how many of them are included within one network for any given "added radius" or particle spacing.

Numerical values for percolation are obtained using a custom C++ program. The classified volume is segmented into discrete objects, which are then dilated by one voxel and segmented again. If two or more particles merge, the new one is given a list of which original particles it contains. This process repeats until there is only a single object remaining. The final data is presented as the largest fraction of the original particles assimilated into any one single object (the percolation fraction) against the particle separation (2 x number of dilate steps x voxel size). Figure 3 is the result of running this procedure on the machine learning-classified volume.

From this, we can see that 25% of the particles percolate at a spacing of 1.3 nm, 50% of the particles percolate at 4.8 nm and 75% of the particles percolate at 16.1 nm. Because these spacings are very close to the voxel size (0.56 nm), it is easy to recognise the importance of accurately classifying the reconstruction.

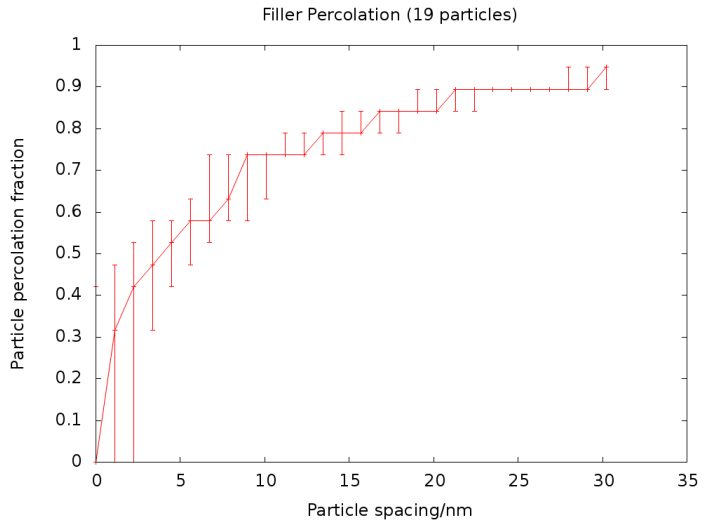

Figure 3: Percolation data from the reconstruction in Figure 2. The volume contained 19 separate particles.

4. Conclusions

We have demonstrated that machine learning methods offer a reliable means of identifying regions of a tomographic reconstruction without using filters to alter the source data or by using time-consuming and potentially inaccurate manual segmentation. Data processed in this manner retains fine details on the order of one or two voxels, meaning that quantitative information can usefully be obtained on particle spacings even when particles approach one another very closely. The next step would be to combine this information with mechanical testing in order to relate the detailed mechanical properties of these rubber composites to the distribution of particle spacings (as opposed to the bulk volume fraction used in current work). Understanding this relationship will allow rubber composite manufacturers to actively design their filler particles in order to more accurately specify and create new materials.

5. Acknowledgements

Funding and rubber composite samples were provided by Michelin. P.A.M. thanks the ERC grant number 291522 '3DIMAGE' for funding.

References

[1] Payne A R 1962 *J. Appl. Polym. Sci.* **6** 57–63 ISSN 1097-4628 URL http://dx.doi.org/10.1002/app.1962.070061906
[2] Kohjiya S, Katoh A, Suda T, Shimanuki J and Ikeda Y 2006 *Polymer* **47** 3298 – 3301 ISSN 0032-3861 URL http://www.sciencedirect.com/science/article/pii/S0032386106002916
[3] Poompradub S, Tosaka M, Kohjiya S, Ikeda Y, Toki S, Sics I and Hsiao B S 2005 *J. Appl. Phys.* **97** 103529 (pages 9) URL http://link.aip.org/link/?JAP/97/103529/1
[4] Wang Z, Liu J, Wu S, Wang W and Zhang L 2010 *Phys. Chem. Chem. Phys.* **12**(12) 3014–3030 URL http://dx.doi.org/10.1039/B919789C
[5] Gilbert P 1972 *Journal of Theoretical Biology* **36** 105 – 117 ISSN 0022-5193 URL http://www.sciencedirect.com/science/article/pii/0022519372901804
[6] Schindelin J, Arganda-Carreras I, Frise E, Kaynig V, Longair M, Pietzsch T, Preibisch S, Rueden C, Saalfeld S, Schmid B, Tinevez J Y, White D J, Hartenstein V, Eliceiri K, Tomancak P and Cardona A 2012 *Nat Meth* **9** 676–682 ISSN 1548-7091 URL http://dx.doi.org/10.1038/nmeth.2019
[7] Breiman L 2001 *Machine Learning* **45** 5–32 ISSN 0885-6125